

---

# Self-Supervision Closes the Gap Between Weak and Strong Supervision in Histology

---

**Olivier Dehaene**

Owkin Inc.

olivier.dehaene@owkin.com

**Axel Camara**

Owkin Inc.

axel.camara@owkin.com

**Olivier Moindrot**

Owkin Inc.

olivier.moindrot@owkin.com

**Axel de Lavergne**

Owkin Inc.

axel.de-lavergne@owkin.com

**Pierre Courtiol**

Owkin Inc.

pierre.courtio1@owkin.com

## Abstract

One of the biggest challenges for applying machine learning to histopathology is weak supervision: whole-slide images have billions of pixels yet often only one global label. The state of the art therefore relies on strongly-supervised model training using additional local annotations from domain experts. However, in the absence of detailed annotations, most weakly-supervised approaches depend on a frozen feature extractor pre-trained on ImageNet. We identify this as a key weakness and propose to train an in-domain feature extractor on histology images using MoCo v2, a recent self-supervised learning algorithm. Experimental results on Camelyon16 and TCGA show that the proposed extractor greatly outperforms its ImageNet counterpart. In particular, our results improve the weakly-supervised state of the art on Camelyon16 from 91.4% to 98.7% AUC, thereby closing the gap with strongly-supervised models that reach 99.3% AUC. Through these experiments, we demonstrate that feature extractors trained via self-supervised learning can act as drop-in replacements to significantly improve existing machine learning techniques in histology. Lastly, we show that the learned embedding space exhibits biologically meaningful separation of tissue structures.

## 1 Introduction

Histopathology is the gold standard for diagnosis in many diseases, and especially in oncology. One example of a routine task performed by pathologists is metastasis detection in hematoxylin and eosin (H&E) stained slides of lymph nodes, which can prove challenging as whole-slide images (WSI) can be over 25 mm wide while micro-metastases can be as small as 50  $\mu m$  wide [2]. However, in most existing cohorts, WSIs are only associated with a pathology report containing global labels, but that lacks detailed pixel-level annotations. In the example above a lymph node slide would only have a binary slide-level label indicating whether it contains any metastasis.

Despite these limitations, recent work has proved that machine learning can perform well on histology images [3], sometimes as well as human experts [4]. Models that attempt to learn directly from global labels belong to the field of *weakly-supervised learning*, and have to propagate the slide-level information down to individual pixels of the WSI. Other models rely instead on additional pixel-level

annotations and are referred as *strongly-supervised*, however these pathologist annotations are costly and time-consuming.

By taking advantage of the added information from annotations, strongly-supervised models perform better than weakly-supervised ones. On Camelyon16 [1], the state of the art for breast cancer metastasis detection is strongly-supervised and reaches an area under the ROC curve (AUC) of 99.3% [35]. Without annotations and despite many recent advances, weakly-supervised learning on Camelyon16 only achieves 91.4% AUC [24]. However, other research questions in histology consist in predicting a label that is not directly visible in the slide, such as the overall survival of the patient [36] or gene expression from transcriptomic data [28]. In these situations, annotations can provide helpful regions of interest but are not enough to solve the task itself, so weakly-supervised learning remains the only option and is therefore a key method for machine learning in histology.

Another challenge for weak supervision is that current constraints on GPU memory prevent full end-to-end learning, as the input WSI itself already takes up to 8GB [27]. Most approaches thus rely on a pre-processing step to reduce the dimensionality of the input, often separating the slide into smaller images (tiles) on which conventional architectures, such as convolutional neural network, can operate. This network, the feature extractor, can be either fine-tuned [11, 23] or frozen [20, 12], but in both cases, the network is often pre-trained on ImageNet [13], an *out-of-domain* dataset of natural images.

We identify the use of out-of-domain pre-training as the main weakness in current weakly-supervised methods. In this paper, we propose to train a new *in-domain* encoder on histology tiles using unsupervised learning. Recent advances [7, 16] have significantly improved the transfer learning performance of unsupervised pre-training. We use one such state-of-the-art self-supervised algorithm, MoCo v2 [9], to train a tile-level feature extractor without supervision. This approach is very well suited to histology, since each WSI contains tens of thousands of unlabeled tiles.

Our work makes the following contributions:

- In Section 3, we propose a generic pipeline combining self-supervised pre-training and weakly-supervised learning.
- We show in Sections 4.1 and 4.2 that our approach is generic enough to yield significant improvements on two datasets for three weakly-supervised algorithms. In particular we close most of the gap between weak and strong supervision on Camelyon16 by reaching 98.7% AUC on the competition test set. In Section 4.3, we bring out the biological relevance of the self-supervised learned features.
- Finally, we demonstrate in Section 4.4 that self-supervised feature extractors can transfer across different organs and tumor types.

## 2 Related Work

**Strong supervision** A number of previous works in histology have relied on pathologists hand-crafted pixel-level annotations to train machine learning models [10, 6, 30]. For tasks like cancer detection, the slide-level label is derived from local tumor annotations: if no tumor is found, the slide-level label is negative. For other tasks, such as molecular subtype prediction, the global label is obtained from external data, such as genomic sequencing, and cannot be expressed as a purely local information. However, in Kather et al. [23] and Sirinukunwattana et al. [31], expert knowledge is added to the model by annotating regions of interest (the tumor area), which may be seen as a weaker form of strong supervision.

**Weak supervision** When annotations are not available, models are trained with weakly-supervised learning using only the slide-level labels as supervision. One of the most common approaches frames the problem as multiple instance learning (MIL) [21]. Weakly-supervised models have been used to predict patient survival in hepatocellular carcinoma [29] or microsatellite instability in colorectal cancer [15].

**End-to-end training on WSI** GPU memory limitations prevent full end-to-end learning on WSIs, and most weakly-supervised approaches use a frozen feature extractor to reduce the input dimension. Pinckaers et al. [26, 27] used a streaming neural network to permit end-to-end training, but at the cost

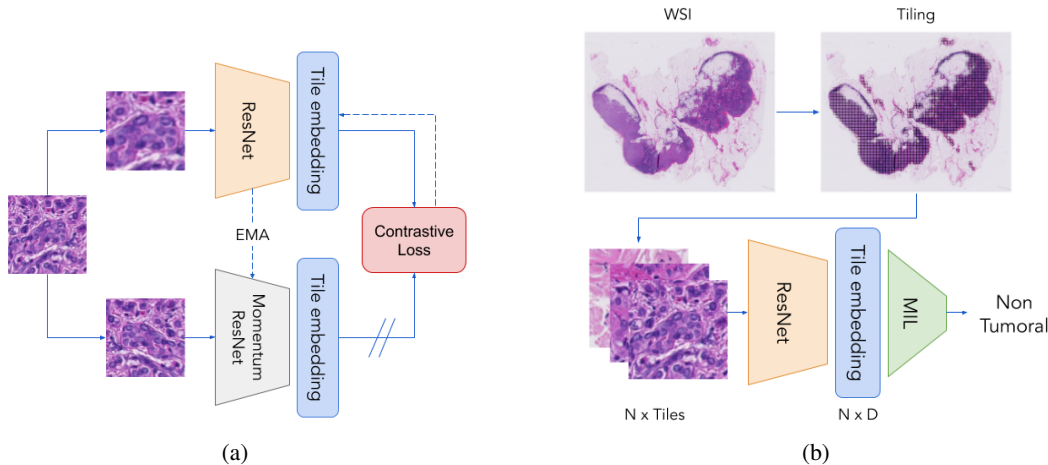


Figure 1: Proposed pipeline. We train a ResNet encoder on histology tiles using MoCo v2, a self-supervised learning algorithm (a) and use the trained encoder as a feature extractor for multiple instance learning (MIL) (b). More details in Section 3.

of only operating on a down-sampled slide 16,384 pixels wide. Campanella et al. [4] used the MIL framework and managed to train their network end-to-end by back-propagating only on the top tiles. Coudray et al. [11] directly used slide-level labels as local tile labels to train their network. Other papers have tried several techniques to pre-train the feature extractor including supervised multitask learning [33] or Bidirectional Generative Adversarial Networks [32].

**Self-supervised algorithms** Over the past two years, rapid developments have been made in the field of self-supervised learning [8, 5]. He et al. [18] showed that self-supervised pre-training outperformed supervised pre-training on ImageNet for downstream transfer learning performance. Among the latest self-supervised algorithms, MoCo v2 [9] can work with smaller batch sizes which makes it a better fit for lower computational resources. Lu et al. [24, 25] applied Contrastive Predictive Coding [34] to histology to pre-train their feature extractor.

### 3 Methods

Our proposed pipeline is summarized in Figure 1. In Section 3.1, we detail the standard workflow for weakly-supervised learning in histology. We then describe in Section 3.2 a generic method to pre-train the feature extractor with self-supervised learning, which can be applied to improve performance in most existing models in histology.

#### 3.1 Weakly-supervised learning in histopathology

To train deep learning models on histology images with only slide-level labels, we use a typical three-step workflow illustrated in Figure 1b: tiling, feature extraction and multiple instance learning training.

**Tiling** We extract from tissue regions a grid of  $N$  tiles of fixed size at a set zoom level, e.g. 0.5 microns per pixel. The total number of tiles  $N$  depends on the tissue area in the WSI.

**Feature extraction** A frozen feature extractor, such as ResNet50 [19] pre-trained on ImageNet, is applied to each of the  $N$  tiles as a pre-processing step. This encoder extracts  $D$  relevant features from each tile. We therefore obtain a matrix of size  $N \times D$  for each slide.

**Multiple Instance Learning** The training phase begins at this step, with an  $N \times D$  matrix as input and a slide-level label as output. In our paper we consider three recent approaches following the multiple instance learning (MIL) framework: Weldon [14], Chowder [12] and DeepMIL [20]. One common attribute of these architectures is that they all first compute an attention score for each tile of

the WSI. In Weldon and Chowder, only the minimum and maximum scores are kept and combined into a final prediction. DeepMIL uses a weighted sum of the tile features using the tile attention scores and computes the prediction using that average representation. Implementation details can be found in Appendix A.

### 3.2 Training a better feature extractor with self-supervised learning

Table 1: Performance for tumor detection (AUC percentage) on Camelyon16 in 5-fold cross-validation (repeated 5 times) on the train set and on the competition test set (5 independent runs). Using the MoCo v2 feature extractor for weakly-supervised learning closes most of the gap with the strongly-supervised state of the art.

Method	Feature Extractor Training Method	Train Cross-Validation	Competition Test Set
<i>Strongly-Supervised</i> [35]	-	-	<b>99.3</b>
CLAM [24]	CPC	-	91.4 ± 2.3
Weldon	ImageNet	76.9 ± 16.6	65.3 ± 13.7
Chowder		82.3 ± 15.4	79.6 ± 5.1
DeepMIL		88.7 ± 4.7	82.9 ± 2.0
Weldon	MoCo V2	97.9 ± 1.4	98.3 ± 0.7
Chowder		<b>98.3 ± 1.2</b>	97.7 ± 0.5
DeepMIL		96.3 ± 2.1	<b>98.7 ± 0.2</b>

As stated before, one key limitation of the approach described in Section 3.1 is the use of a feature extractor trained on out-of-domain data. Here we propose applying recent advances in self-supervised learning to train a better in-domain feature extractor on histology tiles, without annotations.

We use Momentum Contrast v2 (MoCo v2) [9], a self-supervised learning algorithm using contrastive loss to shape an embedding space where different augmented views of the same image are close together. MoCo v2 adds incremental improvements on the original MoCo paper [18]. As shown in Figure 1a, a batch of tile goes through two ResNet encoders with different data augmentations. The contrastive loss then pushes pairs of matching tiles closer, and pairs of different tiles apart. Gradients are only back-propagated through the first of these two encoders. The second encoder is updated with an exponential moving average (EMA) of the first encoder’s weights.

To apply this self-supervised framework on histology data, we concatenate tiles from all WSIs extracted at the tiling step to form a training dataset. We then train the feature extractor with MoCo v2 on this set of unlabeled tile images. We only modify the data augmentation scheme by adding 90° rotations and vertical flips, since histology tiles contain the same information regardless of their orientation. Implementation details can be found in Appendix B.

## 4 Experiments

In this section, we evaluate the performance of our approach on two datasets (Sections 4.1 and 4.2), look at the interpretability of the learned representation (Section 4.3) and its transfer learning potential (Section 4.4).

### 4.1 Metastasis detection on Camelyon16

The Camelyon16 challenge consists in automatically detecting breast cancer metastases in sentinel lymph node WSIs. AUC for 5-fold cross-validation (repeated 5 times) on the train set and AUC on the hold-out test set (5 independent runs) are presented in Table 1.

**Dataset** The Camelyon16 dataset contains a total of 400 sentinel lymph node H&E-stained WSIs from two medical centers, split into 270 for training and 130 for testing. Local annotations done by pathologists at pixel-level for the slides containing metastases are provided.

**Baselines** In Wang et al. [35], a patch-based classifier is trained using local tile annotations and tile predictions are combined in a post-processing stage to establish a strongly-supervised state of the art at 99.3% AUC on the test set. On the other hand, the weakly-supervised learning state of the art achieves 91.4% AUC by pre-training the encoder with Contrastive Predictive Coding [24].

**Results** In our experiments we show that switching from a feature extractor trained on ImageNet to one trained with MoCo v2 on Camelyon16 tiles improves results significantly. We use the exact same parameters for both experiments, only replacing the feature extractor itself. Our best model obtains 98.7% AUC on the test set, setting a new state of the art for weakly-supervised learning on Camelyon16 (+7.3 AUC points compared to Lu et al. [24]), which closes the gap with the strongly-supervised baseline at 99.3% AUC.

We empirically observe performance instability across folds when training Weldon and Chowder on ImageNet features, with standard deviations of 16.6% and 15.4% AUC respectively (Table 1). Courtiol et al. [12] reduced the variability by using an ensemble of 50 models. In our experiments, the standard deviation is divided by a factor of 10 when switching to MoCo v2 features, which demonstrates the robustness and quality of this representation.

## 4.2 Consensus Molecular Subtype classification in colorectal cancer

Table 2: Performance for Consensus Molecular Subtype (CMS) classification (one vs. all AUC percentage for each subtype, and macro average on all subtypes) on TCGA-COAD in 5-fold cross-validation (repeated 5 times). Changing the ImageNet feature extractor to MoCo v2 improves results substantially. Our pipeline obtains comparable results to the state of the art without using tumor annotations, ensembling and additional slides.

Method	Feature Extractor Training Method	CMS1	CMS2	CMS3	CMS4	Macro Average
imCMS [31] *	Tile Classification with Tumor Annotations	85 ± 5	<b>89 ± 3</b>	78 ± 7	<b>83 ± 4</b>	<b>84 ± 3</b>
DeepHistology [22]	ImageNet	70	69	66	60	66.2
Weldon	ImageNet	74.8 ± 7.2	68.9 ± 5.1	66.9 ± 8.4	63.9 ± 7.1	68.6 ± 4.3
Chowder		75.1 ± 7.0	70.9 ± 5.8	64.2 ± 7.6	63.4 ± 6.5	68.4 ± 4.8
DeepMIL		77.4 ± 6.1	74.6 ± 5.7	73.9 ± 6.3	62.5 ± 7.4	72.1 ± 4.0
Weldon	MoCo V2	87.7 ± 4.7	81.9 ± 5.0	<b>82.9 ± 5.0</b>	68.2 ± 5.9	80.1 ± 3.3
Chowder		86.9 ± 5.4	79.9 ± 5.0	79.5 ± 6.4	66.9 ± 6.6	78.3 ± 3.6
DeepMIL		<b>88.2 ± 4.4</b>	82.7 ± 4.0	80.3 ± 5.8	68.8 ± 6.2	80.0 ± 3.5

In this section, we describe results on Consensus Molecular Subtype (CMS) classification on colorectal cancer (Table 2). The AUC is computed with 5-fold cross-validation, repeated 5 times. All models are trained with multiclass classification, and we report one vs. all AUC for each category, as well as the average AUC (Macro Average).

**Dataset** The TCGA-COAD dataset contains a total of 461 colorectal cancer WSIs. Among these, 364 are classified in one of the four transcriptome-based consensus molecular subtypes (CMS) [17].

**Baselines** Sirinukunwattana et al. [31] used additional tumor annotations to train a model called *imCMS* only on tumoral tiles. Although these annotations are not directly linked to the CMS labels, they help the model to focus on meaningful regions of the WSI. Their model is trained on FOCUS, an external cohort of 510 slides and transferred to TCGA-COAD with Domain Adaptation techniques. Kather et al. [22] used a weakly-supervised approach called *DeepHistology* that doesn't use any annotation, but obtain lower results.

**Results** Similarly to results on Camelyon16, switching from ImageNet pre-training to an encoder trained on TCGA-COAD tiles with MoCo v2 increases the AUC by an average of 10 AUC points.

\*Ensemble of 5 models.

Both Weldon and DeepMIL models outperform the state-of-the-art results of *imCMS* in CMS1 (88.2% AUC) and CMS3 (82.9% AUC) subtypes, while using less data, no tumor annotations and no ensembling.

On CMS4, our approach succeeds in increasing the AUC but remains far from the results of Sirinukunwattana et al. [31]. The high infiltration of stromal cells within CMS4 tumors [17] makes it more difficult for the model to focus on the tumor regions. Without local tumor annotations, our weakly-supervised method therefore struggles to accurately detect CMS4 cases.

### 4.3 Interpretability

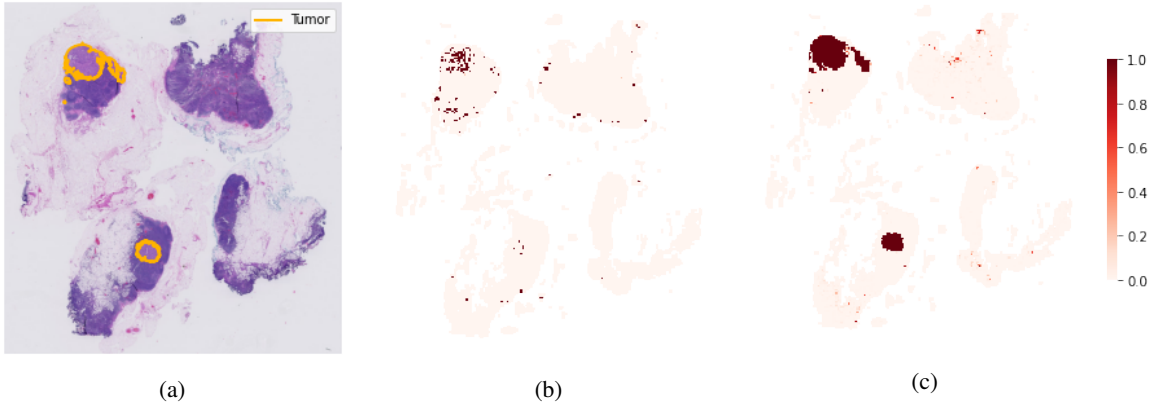


Figure 2: (a) Tumor annotations (orange) displayed on a Camelyon16 test slide. (b) The best performing cluster on ImageNet features among 10 clusters obtains 69.4% AUC. (c) The best performing cluster on MoCoV2 features among 10 clusters obtains 95.1% AUC and matches almost perfectly the annotations, while being fully unsupervised.

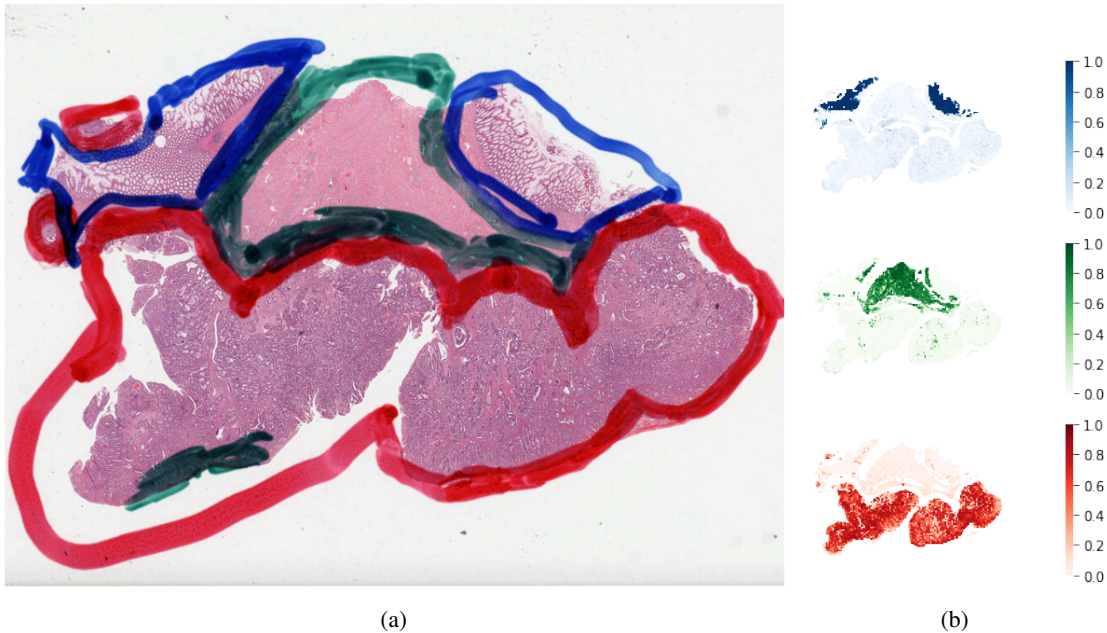


Figure 3: (a) A slide from TCGA-COAD with rough marker annotations. Blue: mucosa with normal intestinal glands, green: muscularis mucosae and submucosa, red: tumoral tissue (b) For each color, the best matching cluster on MoCo v2 features among 10 clusters is displayed.

In this section, we investigate further why the representation of the feature extractor trained with MoCo v2 is better than its ImageNet counterpart, and propose to apply a clustering algorithm to the tile representations. We run K-Means ( $k=10$ ) on the Camelyon16 training tiles features. We find that one of the 10 clusters is highly correlated with the tumoral tiles. As a qualitative test, we take the first slide of the Camelyon16 test set and display in Figure 2 the heatmap of the cluster correlated with the tumoral signal for both ImageNet and MoCo v2 features. We can see how the best unsupervised MoCo v2 cluster for Camelyon16 tiles almost perfectly matches the tumor annotations, while the ImageNet heatmap only covers a portion of the tumor.

We can evaluate quantitatively this correlation using the local annotations provided within the Camelyon16 dataset. To do so, we generate a similarity ranking per cluster by computing the cosine distance between their features and each centroid. We then evaluate this ranking against the tumoral annotations. The best MoCo v2 cluster achieves 95.1% AUC on detecting tumoral tiles, while the same method on ImageNet-encoded tiles only achieves 69.4% AUC. Without any supervision, our MoCo v2 features learn to reliably cluster tumoral tiles.

To test if this method generalizes to other datasets, we apply the same clustering principle to the tiles of TCGA-COAD. Some slides in the dataset contain rough marker annotations, and we display one of them in Figure 3a. Two expert pathologists identified the blue region as mucosa with normal intestinal glands, the green region as muscularis mucosae and submucosa, and the red region as tumoral tissue. Among the 10 tile clusters on MoCo v2 features, we find 3 clusters that match almost perfectly the 3 regions of interest annotated in the slide, as displayed in Figure 3b. We were unable to find meaningful clusters on ImageNet encoded tiles.

The five most representative tiles of each cluster can be seen in Supplementary Figure 1 for Camelyon16 and Supplementary Figure 2 for TCGA-COAD.

#### 4.4 Transfer learning of the feature extractor across datasets

Table 3: Cross-validation performance (AUC percentage) when switching feature extractors on Camelyon16 and TCGA-COAD. For each MIL architecture, we display the performance without transfer learning (on the diagonal) and the performance with transfer of the feature extractor from the other dataset (off diagonal).

MIL Architecture	MoCo v2 Trained On	Metastasis Detection	CMS Classification
Weldon	Camelyon16	$97.9 \pm 1.4$	$68.5 \pm 4.8$
	TCGA-COAD	<b><math>98.2 \pm 1.0</math></b>	<b><math>80.1 \pm 3.3</math></b>
Chowder	Camelyon16	$98.3 \pm 1.2$	$67.4 \pm 4.3$
	TCGA-COAD	<b><math>98.6 \pm 0.9</math></b>	<b><math>78.3 \pm 3.6</math></b>
DeepMIL	Camelyon16	<b><math>96.3 \pm 2.1</math></b>	$74.5 \pm 3.7$
	TCGA-COAD	$94.7 \pm 3.9$	<b><math>80.0 \pm 3.5</math></b>

One drawback of our method is that the training of the self-supervised learning algorithm requires a lot of GPU time. Our Camelyon16 encoder took 13 GPU days to train on 2.6 million tiles. Retraining a new feature extractor for every dataset is not always feasible.

In this section, we investigate how well a feature extractor trained using MoCo v2 is able to transfer across datasets. We benchmark the encoder trained on Camelyon16 on the Consensus Molecular Subtype classification task, and reciprocally the encoder trained on TCGA-COAD on the tumoral classification task. For each task, we do 5 repeated 5-fold cross-validation, resulting in 25 independent runs.

In Table 3, we observe that the feature extractor trained on TCGA-COAD transfers very well to Camelyon16, even outperforming by a small margin the original Camelyon16 feature extractor for the Weldon and Chowder architectures. However, the feature extractor trained on Camelyon16 introduces a significant drop in performance on the CMS prediction task compared to the TCGA-COAD feature extractor. On the CMS classification task, the results of the Camelyon16 feature extractor are on par with results from the ImageNet encoder (Table 2). Campanella et al. [4] experienced a similar drop

in performance ( $-20.2$  AUC points) when transferring a breast cancer metastasis detection model trained on Camelyon16 to an external real-world dataset.

To explain that difference, we hypothesize that the feature extractor trained on TCGA-COAD was able to capture a much more robust representation, as TCGA-COAD contains slides coming from 24 different centers and is closer to a real-world dataset with variations in slide preparation, staining and scanning. On the other hand, the Camelyon16 cohort only comes from 2 different centers and is well curated, which reduces variability. Furthermore, colorectal cancer exhibits a greater variety of histological patterns compared to metastatic lymph nodes.

## 5 Conclusion

Using self-supervision to train the feature extractor, our generic pipeline considerably increases the performance of weakly-supervised learning across three architectures and two datasets, and closes the gap with strongly-supervised models on Camelyon16. An in-domain feature extractor trained with MoCo v2 can therefore act as a drop-in replacement for any histology model currently relying on ImageNet pre-trained networks. Furthermore, the learned embedding space clusters histology tiles into biologically meaningful histological patterns, which could lead to new interactive tools for pathologists to explore WSIs and find novel biomarkers. Finally, by showing transfer learning capabilities, the proposed pipeline lays the foundation for a universal self-supervised histology feature extractor on H&E-stained slides.

## Acknowledgments

We thank Mathieu Andreux, Eric W. Tramel, Charlie Saillard, Alberto Romagnoni, Pierre Manceron, and Aurélie Kamoun for their helpful comments.

We thank the two pathologists Julia Leiner and Vincent Jehanno for validating the results of our clustering model.

This work was granted access to the HPC resources of IDRIS under the allocation 2020-AD011011731 made by GENCI.

The results published here are in part based upon data generated by the TCGA Research Network: <https://www.cancer.gov/tcga>.

## References

- [1] Babak Ehteshami Bejnordi, Mitko Veta, Paul Johannes Van Diest, Bram Van Ginneken, Nico Karssemeijer, Geert Litjens, Jeroen A.W.M. Van Der Laak, Meyke Hermesen, Quirine F. Manson, Maschenka Balkenhol, Oscar Geessink, Nikolaos Stathonikos, Marcory C.R.F. Van Dijk, Peter Bult, Francisco Beca, Andrew H. Beck, Dayong Wang, Aditya Khosla, Rishab Gargeya, Humayun Irshad, Aoxiao Zhong, Qi Dou, Quanzheng Li, Hao Chen, Huang Jing Lin, Pheng Ann Heng, Christian Haß, Elia Bruni, Quincy Wong, Ugur Halici, Mustafa Ümit Öner, Rengul Cetin-Atalay, Matt Berseth, Vitali Khvatkov, Alexei Vylegzhanin, Oren Kraus, Muhammad Shaban, Nasir Rajpoot, Ruqayya Awan, Korsuk Sirinukunwattana, Talha Qaiser, Yee Wah Tsang, David Tellez, Jonas Annuscheit, Peter Hufnagl, Mira Valkonen, Kimmo Kartasalo, Leena Latonen, Pekka Ruusuvoori, Kaisa Liimatainen, Shadi Albarqouni, Bharti Mungal, Ami George, Stefanie Demirci, Nassir Navab, Seiryu Watanabe, Shigeto Seno, Yoichi Takenaka, Hideo Matsuda, Hady Ahmady Phoulady, Vassili Kovalev, Alexander Kalinovsky, Vitali Liauchuk, Gloria Bueno, M. Milagro Fernandez-Carrobles, Ismael Serrano, Oscar Deniz, Daniel Racoceanu, and Rui Venâncio. Diagnostic assessment of deep learning algorithms for detection of lymph node metastases in women with breast cancer. *JAMA - Journal of the American Medical Association*, 318(22):2199–2210, 12 2017.
- [2] Benjamin Bird, Kristi Bedrossian, Nora Laver, Miloš Miljković, Melissa J Romeo, and Max Diem. Detection of breast micro-metastases in axillary lymph nodes by infrared micro-spectral imaging. *Analyst*, 134(6):1067–1076, 2009.
- [3] Wouter Bulten, Hans Pinckaers, Hester van Boven, Robert Vink, Thomas de Bel, Bram van Ginneken, Jeroen van der Laak, Christina Hulsbergen-van de Kaa, and Geert Litjens. Automated deep-learning system for gleason grading of prostate cancer using biopsies: a diagnostic study. *The Lancet Oncology*, 21(2):233–241, Feb 2020.
- [4] Gabriele Campanella, Matthew G. Hanna, Luke Geneslaw, Allen Mirafior, Vitor Werneck Krauss Silva, Klaus J. Busam, Edi Brogi, Victor E. Reuter, David S. Klimstra, and Thomas J. Fuchs. Clinical-grade computational pathology using weakly supervised deep learning on whole slide images. *Nature Medicine*, 25(8):1301–1309, 8 2019.
- [5] Mathilde Caron, Ishan Misra, Julien Mairal, Priya Goyal, Piotr Bojanowski, and Armand Joulin. Unsupervised learning of visual features by contrasting cluster assignments, 2020.
- [6] Lyndon Chan, Mahdi S Hosseini, Corwyn Rowsell, Konstantinos N Plataniotis, and Savvas Damaskinos. Histosegnet: Semantic segmentation of histological tissue type in whole slide images. In *Proceedings of the IEEE International Conference on Computer Vision*, pages 10662–10671, 2019.
- [7] Ting Chen, Simon Kornblith, Mohammad Norouzi, and Geoffrey Hinton. A Simple Framework for Contrastive Learning of Visual Representations. Technical report, 2020.
- [8] Ting Chen, Simon Kornblith, Kevin Swersky, Mohammad Norouzi, and Geoffrey Hinton. Big Self-Supervised Models are Strong Semi-Supervised Learners. Technical report, 2020.
- [9] Xinlei Chen, Haoqi Fan, Ross Girshick, and Kaiming He. Improved Baselines with Momentum Contrastive Learning. Technical report, 2020.
- [10] Dan C Cireşan, Alessandro Giusti, Luca M Gambardella, and Jürgen Schmidhuber. Mitosis detection in breast cancer histology images with deep neural networks. In *International conference on medical image computing and computer-assisted intervention*, pages 411–418. Springer, 2013.
- [11] Nicolas Coudray, Paolo Santiago Ocampo, Theodore Sakellaropoulos, Navneet Narula, Matija Snuderl, David Fenyö, Andre L. Moreira, Narges Razavian, and Aristotelis Tsirigos. Classification and mutation prediction from non-small cell lung cancer histopathology images using deep learning. *Nature Medicine*, 24(10):1559–1567, 10 2018.
- [12] Pierre Courtiol, Eric W. Tramel, Marc Sanselme, and Gilles Wainrib. Classification and Disease Localization in Histopathology Using Only Global Labels: A Weakly-Supervised Approach. 2 2018.
- [13] Jia Deng, Wei Dong, Richard Socher, Li-Jia Li, Kai Li, and Li Fei-Fei. ImageNet: A Large-Scale Hierarchical Image Database. Technical report, 2009.
- [14] Thibaut Durand, Nicolas Thome, and Matthieu Cord. WELDON: Weakly Supervised Learning of Deep Convolutional Neural Networks. Technical report, 2016.
- [15] Amelie Echle, Heike Irmgard Grabsch, Philip Quirke, Piet A van den Brandt, Nicholas P West, Gordon GA Hutchins, Lara R Heij, Xiuxiang Tan, Susan D Richman, Jeremias Krause, et al. Clinical-grade detection of microsatellite instability in colorectal tumors by deep learning. *Gastroenterology*, 2020.
- [16] Jean-Bastien Grill, Florian Strub, Florent Althé, Corentin Tallec, Pierre H Richemond, Elena Buchatskaya, Carl Doersch, Bernardo Avila Pires, Zhaohan Daniel Guo, Mohammad Gheshlaghi Azar, Bilal Piot, Koray Kavukcuoglu, Rémi Munos, and Michal Valko. Bootstrap Your Own Latent A New Approach to Self-Supervised Learning. Technical report, 2020.

- [17] Justin Guinney, Rodrigo Dienstmann, Xin Wang, Aurélien De Reyniès, Andreas Schlicker, Charlotte Sonesson, Laetitia Marisa, Paul Roepman, Gift Nyamundanda, Paolo Angelino, Brian M. Bot, Jeffrey S. Morris, Iris M. Simon, Sarah Gerster, Evelyn Fessler, Felipe De Sousa .E Melo, Edoardo Missiaglia, Hena Ramay, David Barras, Krisztian Homicsko, Dipen Maru, Ganiraju C. Manyam, Bradley Broom, Valerie Boige, Beatriz Perez-Villamil, Ted Laderas, Ramon Salazar, Joe W. Gray, Douglas Hanahan, Josep Taberner, Rene Bernards, Stephen H. Friend, Pierre Laurent-Puig, Jan Paul Medema, Anguraj Sadanandam, Lodewyk Wessels, Mauro Delorenzi, Scott Kopetz, Louis Vermeulen, and Sabine Tejpar. The consensus molecular subtypes of colorectal cancer. *Nature Medicine*, 21(11):1350–1356, 11 2015.
- [18] Kaiming He, Haoqi Fan, Yuxin Wu, Saining Xie, and Ross Girshick. Momentum Contrast for Unsupervised Visual Representation Learning. pages 9726–9735, 11 2019.
- [19] Kaiming He, Xiangyu Zhang, Shaoqing Ren, and Jian Sun. Deep residual learning for image recognition, 2015.
- [20] Maximilian Ilse, Jakub M. Tomczak, and Max Welling. Attention-based deep multiple instance learning. In *35th International Conference on Machine Learning, ICML 2018*, volume 5, pages 3376–3391. International Machine Learning Society (IMLS), 2 2018.
- [21] Maximilian Ilse, Jakub M. Tomczak, and Max Welling. Attention-based deep multiple instance learning. In *35th International Conference on Machine Learning, ICML 2018*, volume 5, pages 3376–3391. International Machine Learning Society (IMLS), 2 2018.
- [22] Jakob Nikolas Kather, Lara R. Heij, Heike I. Grabsch, Chiara Loeffler, Amelie Echle, Hannah Sophie Muti, Jeremias Krause, Jan M. Niehues, Kai A. J. Sommer, Peter Bankhead, Loes F. S. Kooreman, Jefree J. Schulte, Nicole A. Cipriani, Roman D. Buelow, Peter Boor, Nadina Ortiz-Brüchle, Andrew M. Hanby, Valerie Speirs, Sara Kochanny, Akash Patnaik, Andrew Srisuwananukorn, Hermann Brenner, Michael Hoffmeister, Piet A. van den Brandt, Dirk Jäger, Christian Trautwein, Alexander T. Pearson, and Tom Luedde. Pan-cancer image-based detection of clinically actionable genetic alterations. *Nature Cancer*, 1(8):789–799, 8 2020.
- [23] Jakob Nikolas Kather, Alexander T. Pearson, Niels Halama, Dirk Jäger, Jeremias Krause, Sven H. Loosen, Alexander Marx, Peter Boor, Frank Tacke, Ulf Peter Neumann, Heike I. Grabsch, Takaki Yoshikawa, Hermann Brenner, Jenny Chang-Claude, Michael Hoffmeister, Christian Trautwein, and Tom Luedde. Deep learning can predict microsatellite instability directly from histology in gastrointestinal cancer. *Nature Medicine*, 25(7):1054–1056, 7 2019.
- [24] Ming Y. Lu, Richard J. Chen, and Faisal Mahmood. Semi-supervised breast cancer histology classification using deep multiple instance learning and contrast predictive coding (Conference Presentation). In John E. Tomaszewski and Aaron D. Ward, editors, *Medical Imaging 2020: Digital Pathology*, volume 11320, page 18. SPIE, 3 2020.
- [25] Ming Y. Lu, Richard J. Chen, Jingwen Wang, Debora Dillon, and Faisal Mahmood. Semi-Supervised Histology Classification using Deep Multiple Instance Learning and Contrastive Predictive Coding. 10 2019.
- [26] Hans Pinckaers, Wouter Bulten, Jeroen van der Laak, and Geert Litjens. Detection of prostate cancer in whole-slide images through end-to-end training with image-level labels. 6 2020.
- [27] Johannes Henricus Francisca Maria Pinckaers, Bram van Ginneken, and Geert Litjens. Streaming convolutional neural networks for end-to-end learning with multi-megapixel images. *IEEE Transactions on Pattern Analysis and Machine Intelligence*, pages 1–1, 2020.
- [28] Elodie Pronier, Benoît Schmauch, Alberto Romagnoni, Charlie Saillard, Pascale Maillé, Julien Calderaro, Meriem Sefta, Sylvain Toldo, Mikhail Zaslavskiy, Thomas Clozel, et al. He2rna: A deep learning model for transcriptomic learning from digital pathology, 2020.
- [29] Charlie Saillard, Benoît Schmauch, Oumeima Laifa, Matahi Moarii, Sylvain Toldo, Mikhail Zaslavskiy, Elodie Pronier, Alexis Laurent, Giuliana Amaddeo, Hélène Regnault, et al. Predicting survival after hepatocellular carcinoma resection using deep-learning on histological slides. *Hepatology*, 2020.
- [30] Joel Saltz, Rajarsi Gupta, Le Hou, Tahsin Kurc, Pankaj Singh, Vu Nguyen, Dimitris Samaras, Kenneth R Shroyer, Tianhao Zhao, Rebecca Batiste, et al. Spatial organization and molecular correlation of tumor-infiltrating lymphocytes using deep learning on pathology images. *Cell reports*, 23(1):181–193, 2018.
- [31] Korsuk Sirinukunwattana, Enric Domingo, Susan D. Richman, Keara L. Redmond, Andrew Blake, Clare Verrill, Simon J. Leedham, Aikaterini Chatzipli, Claire Hardy, Celina M. Whalley, Chieh Hsi Wu, Andrew D. Beggs, Ultan McDermott, Philip D. Dunne, Angela Meade, Steven M. Walker, Graeme I. Murray, Leslie Samuel, Matthew Seymour, Ian Tomlinson, Phil Quirke, Timothy Maughan, Jens Rittscher, and Viktor H. Koelzer. Image-based consensus molecular subtype (imCMS) classification of colorectal cancer using deep learning. *Gut*, 0:1–11, 7 2020.
- [32] David Tellez, Geert Litjens, Jeroen van der Laak, and Francesco Ciompi. Neural image compression for gigapixel histopathology image analysis. *CoRR*, abs/1811.02840, 2018.

- [33] David Tellez, Geert Litjens, Jeroen van der Laak, and Francesco Ciompi. Neural Image Compression for Gigapixel Histopathology Image Analysis. *IEEE Transactions on Pattern Analysis and Machine Intelligence*, pages 1–1, 8 2019.
- [34] Aäron van den Oord, Yazhe Li, and Oriol Vinyals. Representation learning with contrastive predictive coding. *CoRR*, abs/1807.03748, 2018.
- [35] Dayong Wang, Aditya Khosla, Rishab Gargeya, Humayun Irshad, Andrew H Beck, and Beth Israel. Deep Learning for Identifying Metastatic Breast Cancer. Technical report, 2016.
- [36] Jiawen Yao, Xinliang Zhu, Jitendra Jonnagaddala, Nicholas Hawkins, and Junzhou Huang. Whole slide images based cancer survival prediction using attention guided deep multiple instance learning networks. *Medical Image Analysis*, 65:101789, 2020.

## A Implementation details for MIL algorithms

**Weldon** A set of one dimensional embeddings is computed for the tile features using a multi-layer perceptron (MLP) with 128 hidden neurons. We select R=5 top and bottom scores and average them.

Supplementary Table 1: Weldon implementation details

Layer	Type
1	fc-128
2	fc-1
3	extreme-scores-5
4	average + sigmoid

**Chowder** We use the same parameters as in Courtiol et al. [12]. A set of one dimensional embeddings is computed for the tile features. We select R=5 top and bottom scores and apply a MLP with 200 and 100 hidden neurons and sigmoid activations to the results.

Supplementary Table 2: Chowder implementation details

Layer	Type
1	fc-1
2	extreme-scores-5
3	fc-200 + sigmoid
4	fc-100 + sigmoid
5	fc-1 + sigm

**DeepMIL** A linear layer with 128 neurons is applied to the embedding followed by a Gated Attention layer with 128 hidden neurons. We then apply a MLP with 128 and 64 hidden neurons and ReLU activations to the results.

Supplementary Table 3: DeepMIL implementation details

Layer	Type
1	fc-128
2	gated-attention-128
3	fc-128 + relu
4	fc-64 + relu
3	fc-1 + sigmoid

**Tiling** In our experiments, we extract from each WSI a maximum of 10,000 tiles of size  $224 \times 224$  at a zoom level of 0.5 microns per pixel. When the WSI contains less than 10,000 tiles we take all tiles available, otherwise we randomly sample 10,000 tiles.

**Optimization details** We train for 15 epochs with a batch size of 16 using Adam with a learning rate of 0.001, betas=(0.9, 0.999), epsilon=1e-8 and no weight decay.

## B Implementation details for MoCo v2

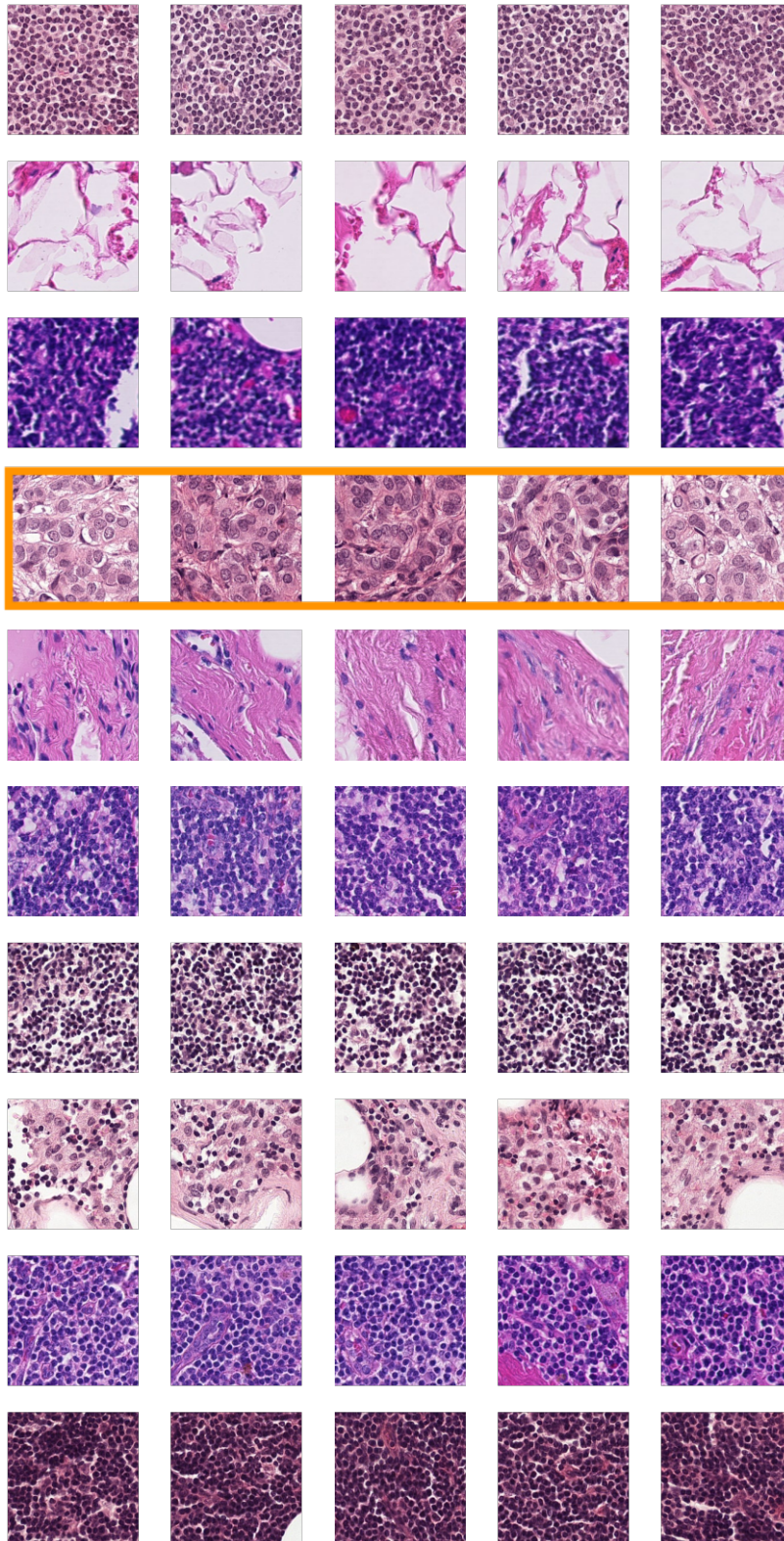
Supplementary Table 4: MoCo v2 data augmentation details

Type	Parameters
RandomRotate	90°, 170°, 280°
RandomVerticalFlip	-
RandomHorizontalFlip	-
RandomResizedCrop	scale=(0.2, 1.0)
ColorJitter	brightness=0.8 contrast=0.8 saturation=0.8 hue=0.2
RandomGrayscale	-
GaussianBlur	sigma_min=0.1 sigma_max=2.0

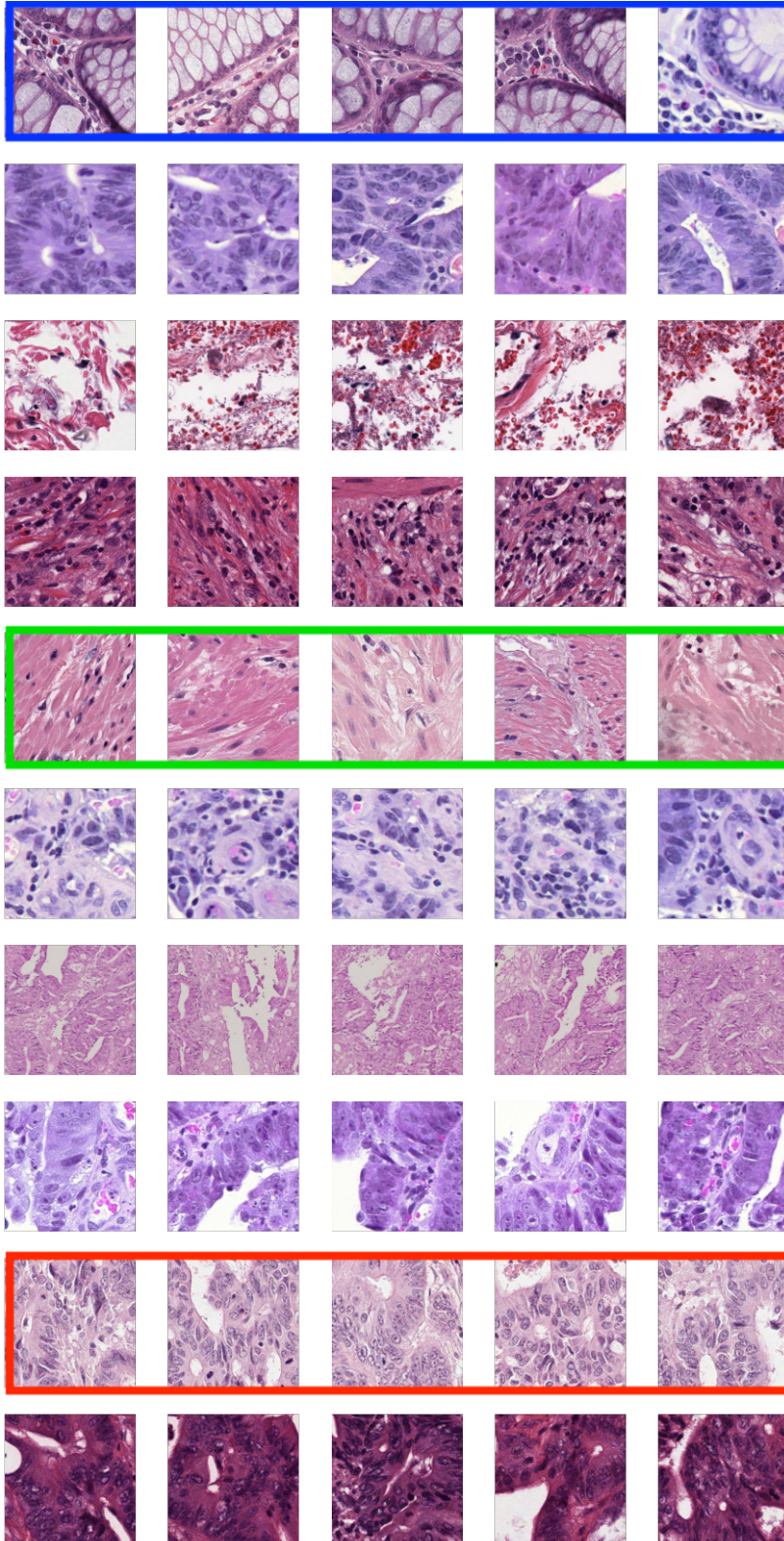
**Training dataset** For each WSI in the cohort, we extract a maximum of 10,000 tiles of size  $224 \times 224$  at a zoom level of 0.5 microns per pixel. When the WSI contains less than 10,000 tiles we take all tiles available, and we otherwise randomly sample 10,000 tiles. The training dataset on Camelyon16 contains 2,646,426 million tiles, while the one on TCGA-COAD contains 2,486,159 million tiles.

**Data augmentation** The data augmentation pipeline used during training is described in Supplementary Table 4.

**Optimization** We train for 200 epochs with a batch size of 4,096 over 16 NVIDIA Tesla V100. We use the LARS optimizer with a learning rate of 0.2, momentum of 0.9, weight decay of  $1.5e-6$  and eta of  $1e-3$ .



Supplementary Figure 1: The five most representative tiles of each of the 10 clusters found in the Camelyon16 tile embedding for MoCo v2. In orange, tumoral tissue. Please refer to Figure 2c for an example of this cluster overlaid on a Camelyon16 slide.



Supplementary Figure 2: The five most representative tiles of each of the 10 clusters found in the TCGA-COAD tile embedding for MoCo v2. In blue, mucosa with normal intestinal glands. In green, muscularis mucosae and submucosa. In red, tumoral tissue. Please refer to Figure 3b for an example of these three clusters overlaid on a TCGA-COAD slide.